University of South Carolina
Scholar Commons

Faculty Publications | Earth, Ocean and Environment, School of the

12-2000

A Simple Surface Temperature Assimilation Scheme for Use in Land Surface Models

Venkataraman Lakshmi
University of South Carolina - Columbia, vlakshmi@geol.sc.edu

Follow this and additional works at: https://scholarcommons.sc.edu/geol_facpub

 Part of the Earth Sciences Commons

Publication Info

Published in *Water Resources Research*, Volume 36, Issue 12, 2000, pages 3687-3700.
Lakshmi, V. (2000). A simple surface temperature assimilation scheme for use in land surface models. *Water Resources Research, 36* (12), 3687-3700.
© Water Resources Research 2000, American Geophysical Union

This Article is brought to you by the Earth, Ocean and Environment, School of the at Scholar Commons. It has been accepted for inclusion in Faculty Publications by an authorized administrator of Scholar Commons. For more information, please contact digres@mailbox.sc.edu.

WATER RESOURCES RESEARCH, VOL. 36, NO. 12, PAGES 3687–3700, DECEMBER 2000

A simple surface temperature assimilation scheme for use in land surface models

Venkataraman Lakshmi
Department of Geological Sciences, University of South Carolina, Columbia

Abstract. This paper examines the utilization of surface temperature as a variable which can be assimilated in off-line land surface hydrological models. The connection between the surface temperature and evapotranspiration is utilized in making adjustments to the model-computed surface soil moisture. This adjustment is a function of the difference between the model-computed and the observed surface temperature. Comparisons between the model-computed and satellite-observed surface temperatures have been carried out. The assimilation of surface temperature is carried out twice a day (corresponding to the A.M. and P.M. overpass of the NOAA 10) over the Red-Arkansas basin in the southwestern United States (31°50'N–36°N, 94°30'W–104°30'W) for a period of 1 year (August 1987 to July 1988). The soil moisture estimates resulting from the assimilation of surface temperature have a closer agreement with the values derived from the special sensor microwave imager than those from simulations without surface temperature assimilation. Assimilation reduces the effect of errors in precipitation and/or shortwave radiation on simulated soil moistures.

1. Introduction

Land surface modeling has faced limitations in the past because of the lack of observations of spatially distributed data of land surface characteristics as well as variables in water and energy budgets, namely, surface temperature and soil moisture. The problem of spatially distributed land surface characteristics has been solved with the advent of the soils database (Continental United States, State Soil Geographic Database (CONUS-SOIL, STATSGO) [*Miller and White*, 1998]) and the global vegetation index (GVI) [*Goward et al.*, 1994]). Surface temperature observations are available from various satellite sensors: advanced very high resolution radiometer (AVHRR) [*Price*, 1984], geostationary orbiting Earth Satellite (GOES) [*Diak*, 1990], and TIROS operational vertical sounder (TOVS) [*Susskind et al.*, 1997]. However, soil moisture still remains as an underobserved hydrologic variable.

Soil moisture is a crucial component of both the water and energy budget equations. The absence of spatially distributed observations of soil moisture makes it very difficult for hydrological model validation. Comparison of model-computed streamflows at the catchment outlet with the observed streamflow does not ensure a complete energy and water budget validation. There could be compensating errors in the infiltration, evaporation, and streamflow which could offset each other and thereby attain proper water balance, but the individual components (infiltration, evaporation, streamflow, and soil moisture) could still be incorrect. It is therefore imperative to use other data sets to ensure the spatially distributed validity of the output of these models as well as the validity of the individual components of the water and energy budgets.

Satellite-observed surface temperatures satisfy our requirements of being spatially distributed and having connections to both the water and the energy budgets. Surface temperature influences evapotranspiration (because of the dependence of the saturation vapor pressure on the surface temperature) and hence the energy budget. Evapotranspiration is connected to the water budget as it determines the subtraction of moisture from the soil layers.

However, comparisons of surface temperature still do not ensure that the model simulations of surface soil moisture are accurate. There are various reasons for inaccuracies in the modeled soil moisture. The primary reason is the errors in the forcing inputs of precipitation and incoming solar radiation. The problems faced by global climate models in simulating precipitation have been documented in the Atmospheric Model Intercomparison Project [*Gates et al.*, 1999]. In addition, intercomparison of land surface model outputs derived using similar forcing data has yielded information on the inadequacies of various parameterizations [*Henderson-Sellers et al.*, 1996].

Therefore we need to compensate for the errors in the input forcings by assimilating the readily available spatially distributed satellite-observed surface temperatures. The model surface temperatures will be adjusted so as to reduce their differences with the observed surface temperatures. These adjustments will be carried out such that the soil moistures are corrected to correspond to the new surface temperatures so that they obey the water and energy budget equations.

The subject of assimilation of soil moisture or other meteorological variables in order to estimate soil moisture accurately is a relatively new area of study [*McLaughlin*, 1995]. Recent advances in inverse methods [*Entekhabi et al.*, 1994; *Lakshmi et al.*, 1997b] have demonstrated the use of microwave satellite data in estimating soil moisture. The assimilation of soil moisture from low-level atmospheric variables using a mesoscale model [*Bouttier et al.*, 1993a, 1993b] has shown that the assimilated soil moisture estimates help in the initialization of atmospheric models. Another class of methods use satellite estimates of surface temperature [*Ottle and Vijal-Majdar*, 1994] and surface temperature tendencies [*McNider et al.*, 1994] to

Copyright 2000 by the American Geophysical Union.

Paper number 2000WR900204.
0043-1397/00/2000WR900204$09.00

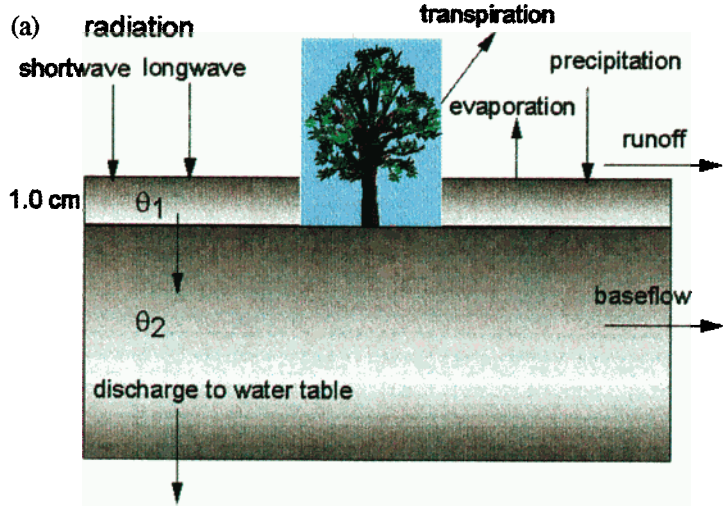

(b)

0.12	3.92	4.77	0.28	1.37	5.26	4.36	0.44	7.09	3.2	2.41
0.47	2.39	1.46	1.6	0.04	4.56	2.16	0.83	0.99	1.72	1.26
0.29	2.16	2.43	3.77	1.19	5.15	2.13	1.67	2.62	2.4	0.07
0.93	2.12	5.6	5.61	4.38	5.98	0.82	1.29	5.56	1.61	0.46
-0.61	2.14	4.8	3.02	6.27	2.27	-0.1	0.2	0.64	0.26	0.5
1.64	1.95	0.78	0.75	4.7	4.45	2.08	-0.46	-0.3	-0.21	-0.15

Perfect Inputs (control)

0.12	3.95	4.8	0.3	1.34	5.33	5.37	0.57	7.12	3.28	2.5
0.48	2.46	1.41	1.6	0.07	4.57	2.14	0.71	1.01	1.76	1.3
0.3	2.2	2.45	3.76	1.21	5.44	2.12	1.75	2.6	2.42	0.11
0.93	2.12	5.73	5.63	4.48	6.13	0.91	1.1	5.73	1.77	0.47
-0.61	2.19	4.99	2.99	6.33	2.19	-0.08	0.36	0.54	0.14	0.51
1.62	2.13	0.76	0.78	4.56	4.68	2.1	-0.45	-0.39	-0.21	-0.12

-20% Rainfall Input Bias

0.13	3.88	4.74	0.26	1.46	5.21	4.24	0.44	6.99	3.12	2.32
0.45	2.34	1.42	1.58	0.02	4.43	2.17	1.06	0.98	1.66	1.25
0.3	2.12	2.41	3.73	1.14	5	2.15	1.62	2.61	2.36	0.02
0.92	2.11	5.42	5.59	4.12	5.9	0.79	1.19	5.47	1.55	0.43
-0.59	2.09	4.56	3.02	6.17	2.31	-0.11	0.08	0.66	0.37	0.5
1.63	1.82	0.76	0.73	4.76	4.25	2.01	-0.47	-0.23	-0.21	-0.15

+20% Rainfall Input Bias

Color Table

< 0	0-3	3-6	> 6

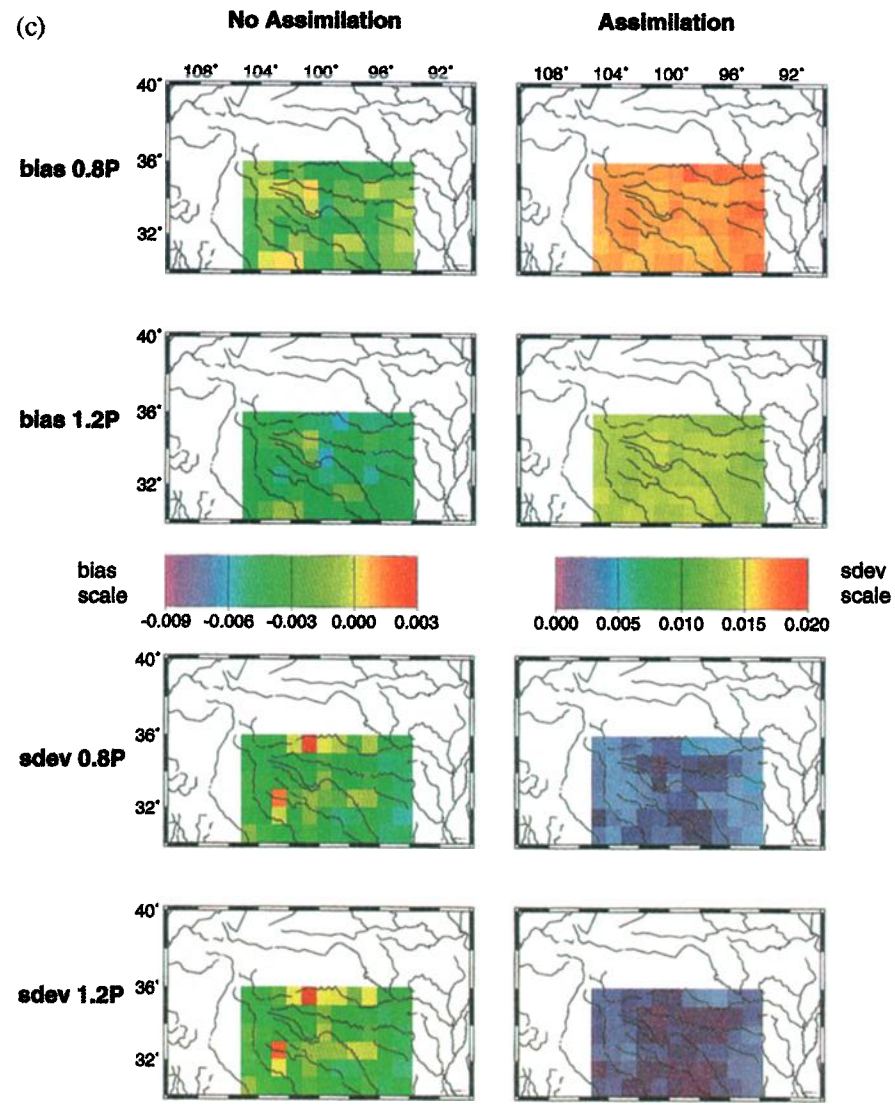

Plate 1. (a) Water and energy balance in the land surface hydrology model. (b) Cumulative difference (in millimeters) between the surface soil moisture derived from the special sensor microwave imager (SSM/I) and the hydrological model simulated without assimilation of surface temperature and the surface soil moisture from SSM/I and the hydrological model simulated with assimilation of surface temperature for November 1987 to August 1988. (c) Spatial distribution of the volumetric upper layer soil moisture bias (control with assimilation, perturbed rainfall input with and without assimilation) and the standard deviation of the bias for the period between August 1, 1987, and July 31, 1988.

adjust for the soil moisture and estimate with greater accuracy the surface fluxes and surface temperature. *van den Hurk et al.* [1997] carry out assimilation by nudging the forecast model evaporation fraction using the satellite data and hydrological model–computed evaporative fraction. The results are reductions in the predicted 2-m air temperature and vapor pressure after carrying out these assimilations. Parameterization of hydrological models using microwave satellite data [*Blyth*, 1993] has proved to be helpful. Our method of surface temperature assimilation is quite similar to the methods of *Ottle and Vijal-Majdar* [1994] and *McNider et al.* [1994], who have used surface temperature to adjust the model-simulated soil moisture. However, *Ottle and Vijal-Majdar* [1994] did not carry out distributed comparisons for their scheme. They compared the daily discharges between the assimilated and the unassimilated cases and point soil moisture comparisons for a few sites. The study by *McNider et al.* [1994] was carried out for a limited time period (few hours to few days) and did not fully validate (over an extended time period) the improvements due to assimilation of surface temperature. This method differs from the scheme of *Bouttier et al.* [1993a, 1993b], who use a regression between soil moisture and air temperature and relative humidity.

In this paper, the model-computed surface temperature and the satellite-observed surface temperatures will be compared. The effect of assimilation in removing the errors caused by incorrect input forcings will be studied. Spatially distributed comparisons are carried out over an area (roughly 5° latitude × 10° longitude) and a time period of a year between the assimilated and the unassimilated scenarios. In this paper, we have carried out assimilation of satellite surface temperatures. However, this methodology is completely general to be applied with field measurements of surface temperature.

2. Theory

The land surface hydrology can be represented by a two-layer model (top layer is 1-cm thick and the bottom layer is 99-cm thick), as shown in Plate 1a [*Mahrt and Pan*, 1984; *Lakshmi et al.*, 1997a]. The water balance for the model can be written as

$$z_1 \frac{\partial \theta_1}{\partial t} = P - E - R - q_{1,2},$$

$$z_2 \frac{\partial \theta_2}{\partial t} = q_{1,2} - q_{2,wt} - T, \tag{1}$$

where θ_1 and θ_2 are the volumetric soil moistures of the top layer (with thickness z_1) and the bottom layer (with thickness z_2), respectively. P is the precipitation, E is the bare soil evaporation, R is the surface runoff, T is the transpiration, $q_{1,2}$ is the moisture flow from layer 1 to layer 2 and $q_{2,wt}$ is the moisture flow from layer 2 to the water table. The time step in this model is 1 hour. In this model the transpiration is assumed to occur from the bottom layer only. The moisture flow from layer 1 to layer 2 ($q_{1,2}$) and the flow from layer 2 to the water table ($q_{2,wt}$) are modeled using Richard's equation accounting for the gravity advection and the moisture gradient. The bare soil evaporation and the vegetation transpiration are estimated using the supply and demand principle; that is, if there is enough moisture to satisfy the potential value, evaporation and transpiration occur at the potential rate, else they occur at a rate limited by the amount of available soil moisture.

The energy balance equation for the land surface (which is used to calculate the surface temperature T_s) is written as a balance between the net radiation and sensible, latent, and ground heat fluxes as

$$R_{sd}(1 - \alpha) + R_{ld} - \varepsilon\sigma T_s^4 - \frac{\rho C_p}{\gamma(r_{av} + r_c)}(e_s(T_s) - e_a)$$

$$- \frac{\rho C_p}{r_{ah}}(T_s - T_a) - \frac{\kappa}{D}(T_s - T_d) = 0, \tag{2}$$

where R_{sd} and R_{ld} are the incoming shortwave and longwave radiation, respectively, and α, ε, and σ are the albedo, emissivity, and the Stefan-Boltzmann's constant, respectively. ET is the evapotranspiration flux, equal to E plus T; T_s, T_a, and T_d are the surface temperature, air temperature, and the deep soil (50 cm) temperature, respectively. Variables $e_s(T_s)$ and e_a are the saturated vapor pressure at surface temperature T_s and actual vapor pressure of the air, respectively. Variables ρ, C_p, and γ are the density, specific heat, and psychrometric constant of air; r_{av} and r_{ah} are the aerodynamic resistances to vapor and heat, respectively, and r_c is the canopy resistance. Variables κ and D are the thermal conductivity and the diurnal damping depth of the soil. The aerodynamic resistances to vapor (r_{av}) and heat (r_{ah}) are taken as equal to each other and are evaluated as [*Brutsaert*, 1982]

$$r_{av} = r_{ah} = \frac{1}{k^2 u}\left[\ln\left(\frac{z - d}{z_0}\right)\right]^2, \tag{3}$$

where k is the von Karman constant (0.4), u is the wind speed, at elevation z, z_0 is the roughness length, and d is the zero plane displacement. The canopy resistance is given by [*Feyen and Hillel*, 1980]

$$r_c = r_{\min}^{st}/\Omega, \tag{4}$$

where $r_{\min}^{st}$ is the minimum stomatal resistance and Ω is the leaf area index. The depth of the top layer of the soil was set to be 1 cm in order to evaluate the surface temperature and the surface soil moisture.

2.1. Assimilation of Surface Temperature

Evapotranspiration is the common variable that couples the land surface water and energy balance equations. Changes in the surface temperature of the land surface alter the heat fluxes, net radiation and latent, sensible, and ground heat fluxes. The change in latent heat flux or evapotranspiration changes the soil moisture content of the layers contributing to the evaporation (from the 1-cm layer) and the transpiration (from the 99-cm layer). Therefore the assimilation of surface temperature changes the soil moisture.

Let T_s^m be the surface temperature computed by the land surface model and T_s^o be the satellite-observed surface temperature. As stated earlier, the observed surface temperature can be ground in situ observations and/or satellite observations. In this study, we used satellite-retrieved surface temperatures for the observations. As a starting point, let us assume that these two estimates of surface temperature can be combined algebraically in a simple fashion to obtain the "correct" estimate of the surface temperature. One way of combining these two estimates to yield an assimilated surface temperature estimate would be

$$T_s' = \frac{(\Delta T_s^o)^2}{(\Delta T_s^m)^2 + (\Delta T_s^o)^2} T_s^m + \frac{(\Delta T_s^m)^2}{(\Delta T_s^m)^2 + (\Delta T_s^o)^2} T_s^o, \tag{5}$$

where ΔT_s^o and ΔT_s^m are the errors in the observed surface temperature and the model-simulated surface temperature, respectively, assuming the errors are uncorrelated.

In reality, both the error associated with the model estimate of surface temperature as well as the observed surface temperature are difficult to determine. As a result, in this paper a simple average is used to estimate T_s' as follows:

$$T_s' = \frac{T_s^o + T_s^m}{2}. \tag{6}$$

In section 5 I will present a more detailed explanation for the choice of using a simple average in (6). This choice is relative to the magnitude of the differences of the model-estimated T_s and the field measurement of T_s and the magnitude of the satellite-retrieved T_s and the field measurement of T_s.

The assimilated surface temperature T_s' will have to satisfy the energy balance equation. Therefore we can calculate the value of the evapotranspiration flux ET′ that satisfies the same (from (2)), i.e.,

$$\mathrm{ET}' = R_{sd}(1 - \alpha) + R_{ld} - \varepsilon\sigma T_s'^4 - H_1(T_s' - T_a) - G_1(T_s' - T_d), \tag{7}$$

where ET′ is the new evapotranspiration flux associated with the assimilated surface temperature T_s' and H_1 and G_1 are the coefficients dependent on the aerodynamic resistance to heat flux and soil resistance to heat conduction, respectively; $H_1 = \rho C_p / r_{ah}$ and $G_1 = \kappa/D$. ET′ is a combination of the bare soil evaporation and the vegetation transpiration (in depth units); we have

$$\frac{\mathrm{ET}'}{\rho_w L} = \frac{E'}{\rho_w L} + \frac{T'}{\rho_w L}, \tag{8}$$

where ρ_w and L are the density and latent heat of evaporation for water, respectively. This new bare soil evaporation E' and vegetation transpiration T' are given by partition based on weighting the thickness of the two soil layers, i.e.,

$$E' = \mathrm{ET}' \frac{W_1}{W_1 + W_2}, \qquad T' = \mathrm{ET}' \frac{W_2}{W_1 + W_2}. \tag{9}$$

W_1 and W_2 are the water-holding capacities of layer 1 and layer 2, respectively, along with the assumption that the bare soil evaporation E occurs from layer 1 only and the vegetation transpiration T occurs from layer 2 only (no roots in layer 1). The difference between the model-computed and the new evapotranspiration flux ET′ is given by

$$\mathrm{ET}' - \mathrm{ET} = \delta\mathrm{ET} = -4\varepsilon\sigma T_s^3 \delta T_s - H_1 \delta T_s - G_1 \delta T_s, \tag{10}$$

where $\delta T_s = T_s' - T_s$, the difference between the assimilated surface temperature and the model-computed surface temperature. The partition of this difference in evapotranspiration δET into the difference for bare soil evaporation δE and the vegetation transpiration δT is given by

$$\delta E = \delta\mathrm{ET} \frac{W_1}{W_1 + W_2}, \qquad \delta T = \delta\mathrm{ET} \frac{W_2}{W_1 + W_2}. \tag{11}$$

The soil moisture of layer 1 and layer 2 has to be modified by $\delta\theta_1$ and $\delta\theta_2$, respectively, when this new bare soil evaporation and vegetation transpiration are implemented, i.e.,

$$\delta\theta_1 = \frac{\delta E}{\rho_w L} \frac{\Delta t}{z_1}, \qquad \delta\theta_2 = \frac{\delta T}{\rho_w L} \frac{\Delta t}{z_2}, \tag{12}$$

where Δt is the time step in our land surface model. We will adjust the layer 1 soil moisture by $\delta\theta_1$ and the layer 2 soil moisture by $\delta\theta_2$ as

$$\theta_1' = \theta_1 + \delta\theta_1, \qquad \theta_2' = \theta_2 + \delta\theta_2. \tag{13}$$

Here θ_1' and θ_2' are the new soil moistures associated with the assimilated surface temperature T_s'; they are physically consistent with the energy and water balance.

This method is completely general; it does not depend on the thickness of the soil layers or the parameterizations used in the land surface model. Given an assimilated surface temperature, the land surface soil moisture is changed to keep the energy and water budgets balanced. Therefore at no stage is the conservation of energy or water violated.

2.2. Impact of Surface Temperature Assimilation

In order to investigate the impact of the surface temperature assimilation on model-simulated soil moisture using the above procedure, we have performed computations for a few scenarios. Corresponding to surface temperatures T_s of 273, 283, 293, 303, 313, and 323 K, the energy balance factor $\mathrm{EB}_f = 4\varepsilon\sigma T_s^4 + H_1 + G_1$ is computed for a 2-m wind speed of 4.0 m s^{-1}, zero plane displacement of 0.25 m, roughness length of 0.07 m, thermal conductivity of 3.5 J s^{-1} m^{-1} K^{-1}, and diurnal damping depth of 0.5 m. We calculate the corrections in soil moisture $\delta\theta_1$ and $\delta\theta_2$ as follows:

$$\delta\theta_1 = (\delta T_s)(\mathrm{EB}_f) \frac{1}{z_1} \frac{W_1}{W_1 + W_2} \frac{\Delta t}{\rho_w L}, \qquad \delta\theta_2 = (\delta T_s)(\mathrm{EB}_f) \frac{1}{z_2} \frac{W_2}{W_1 + W_2} \frac{\Delta t}{\rho_w L}. \tag{14}$$

We have chosen in our model $z_1 = 1.0$ cm and $z_2 = 99.0$ cm. Using a residual soil moisture content θ_r of 0.02 and saturated soil moisture content θ_s of 0.50, $W_1 = (0.50\text{–}0.02)1.0 = 0.48$ cm and $W_2 = (0.50\text{–}0.02)99.0 = 47.52$ cm and the factors $(1/z_1)[W_1/(W_1 + W_2)]$ and $(1/z_2)[W_2/(W_1 + W_2)]$ are equal to 1.0 m^{-1}. This is a result of our choice of a hydrological model with a thin top layer of 1.0 cm and a bottom layer of 99.0 cm. As a result of this simplification, (14) is identical for $\delta\theta_1$ and $\delta\theta_2$ as

$$\delta\theta_1 = \delta\theta_2 = (\delta T_s)(\mathrm{EB}_f) \frac{\Delta t}{\rho_w L}. \tag{15}$$

The values for ρ_w and L are 997 kg m^{-3} and 2500 K J kg^{-1}, and Δt is 1 hour. Using the above expressions and the above values, the energy balance factor EB_f for the surface temperature range 273–323 K is 85.44–88.41 W m^{-2} K^{-1} and $\delta\theta_1/\delta T_s$ and $\delta\theta_2/\delta T_s$ equal to each other are in the range 1.23×10^{-4}–1.28×10^{-4} K^{-1}. This result shows that the impact of the

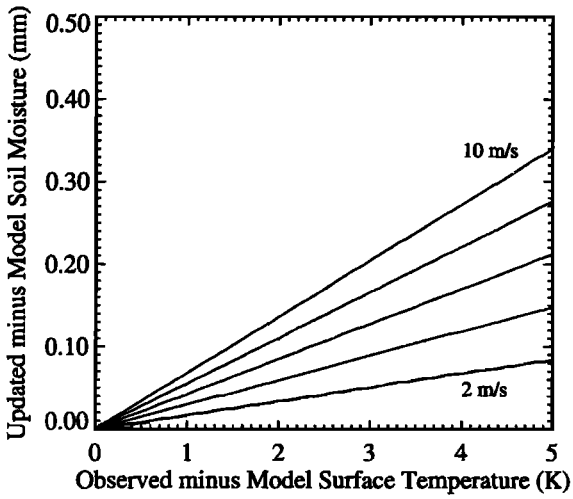

Figure 1. Adjustment in the upper soil moisture amount (millimeters) corresponding to a single day difference in model-simulated and observed surface temperature.

Table 1. List of Surface Airways Stations

Name	Latitude	Longitude	Height, feet[a]
Abilene, Texas	32°25′	99°41′	21
Amarillo, Texas	35°14′	101°42′	23
Dallas-Fort Worth, Texas	32°54′	97°02′	22
Lubbock, Texas	33°39′	101°49′	25
Midland, Texas	31°57′	102°11′	22
Oklahoma City, Oklahoma	35°24′	97°36′	20
Roswell, New Mexico	33°18′	104°32′	20
Stephenville, Texas	32°13′	98°11′	20
Wichita Falls, Texas	33°58′	98°29′	21
Longview, Texas	32°21′	94°39′	22
Tucumcari, New Mexico	35°11′	103°36′	22
San Angelo Mathis, Texas	31°22′	100°30′	20
Clayton, New Mexico	36°27′	103°09′	33
Fort Smith, Arkansas	35°20′	94°22′	23
Dodge City, Kansas	37°46′	99°58′	33
El Paso, Texas	31°48′	106°24′	32
Lufkin Angelina, Texas	31°14′	94°45′	22

[a]One foot equals 0.3048 m.

difference in surface temperature of the model and assimilation (δT_s) on the volumetric soil moisture content is very small. In the case of a 10 K difference in surface temperature the adjustment in the volumetric soil moisture contents $\delta\theta_1$ and $\delta\theta_2$ is 0.00125. This translates into a soil water depth of 0.00125 cm for layer 1 and 0.124 cm for layer 2. This is the adjustment incurred in per model time interval (1 hour in this case). In case the difference between the model and the assimilated surface temperature is on the average 3 K for each hour for 10 days, the adjustment to the volumetric soil moisture contents is 0.09. The corresponding adjustment to the total soil water depths is 0.09 cm in layer 1 and 8.9 cm in layer 2. The variation in the soil moisture content increment (in millimeters) for the top layer with δT_s is shown in Figure 1 for various wind speeds (2 m s^{-1}–10 m s^{-1} at increments of 2 m s^{-1}). The variation of the surface soil moisture increment with δT_s is linear. Figure 2 shows that as the wind velocity increases, the changes in the soil moisture for the same δT_s also increase.

3. Comparisons of Surface Temperature

3.1. Description of Study Area

This study was carried out over an areal extent of 4.75° in latitude and 10.5° in longitude in the southwestern plains of United States (Figure 2). The area includes a small part of eastern New Mexico, most of Oklahoma (except a small part in the north), and northern Texas (a small portion of the panhandle is left out). The region has a topographic relief between 600 and 1500 m in the high plains of eastern New Mexico and western Texas, between 300 and 600 m in midcontinent plains of north central Texas and central Oklahoma, between 150 and 300 m in eastern Oklahoma, and between 0 and 150 m in the Gulf Atlantic rolling plains of southeastern Texas. The vegetation ranges from grama buffalo grass in eastern New Mexico and western Texas to mesquite buffalo grass in south central Texas, cross timbers in north central Texas, and oak hickory pine forests in southeastern Oklahoma and eastern Texas. The land types in the area include subhumid grassland, semiarid grazing land, cropland, irrigated land, cropland pasture, woodland, and forests. The mean annual precipitation ranges from around 40 cm in the western regions to 120 cm in the eastern regions of the study area.

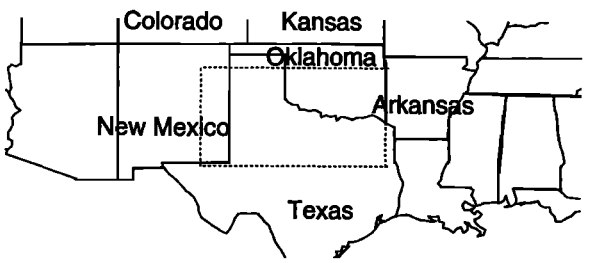

Figure 2. Grid box of study area in the Red-Arkansas study region.

3.2. Data Sets

The meteorological data were obtained from the surface airways stations (17 stations on a hourly temporal frequency) from EarthInfo's National Climate Data Center data product. These data were used to force the model. The meteorological variables include: air temperature, dew point temperature, air pressure, wind speed, cloud height (defined as the height of the lowest sky cover layer more than 1/2 opaque), total sky cover, and wind speed. Table 1 gives a list of the surface airways stations as well as their geographical location. The incoming longwave radiation (I_l) is computed using $I_l = KE_a\sigma T_a^4$, where K is a factor that accounts for cloud cover effects and is given by $K = 1 + 0.17N^2$ [*Tennessee Valley Authority*, 1972], N is the fraction of the sky covered by clouds, E_a is the atmospheric emissivity given by [*Idso*, 1981] $E_a = 0.740 + 0.0049e$, e is the vapor pressure in millibars, σ is the Stefan Boltzmann constant (5.67×10^{-8} J m^{-2} s^{-1} K^{-4}), and T_a is the surface air temperature. The incoming clear-sky shortwave radiation is based on the digital elevation map of the area [*Dozier and Frew*, 1990]. This value is corrected for cloud cover effects [*Eagleson*, 1970] by the factor $1 - (1 - K)N$ to obtain the corrected incoming shortwave radiation; K accounts for the cloud height ($K = 0.18 + 0.0853z$, where z is cloud base altitude in kilometers).

The vegetation data have been obtained from the University

of Maryland reprocessed National Oceanic and Atmospheric Administration (NOAA) Global Vegetation Index Data Product [*Goward et al.*, 1994] from measurements made by AVHRR onboard NOAA polar-orbiting satellites. The observations were mapped to a plate carree' projection (between 75°N and 55°S, with a resolution of 16 km at the equator) and calibrated radiometrically for spectral reflectance. The normalized difference vegetation index (NDVI) values were converted to leaf area index (Ω) using a Beer's law kind of variation [*Baret and Guyot*, 1991] as NDVI = NDVI_∞ + (NDVI_g − NDVI_∞) exp ($-K_{\text{NDVI}}\Omega$), where NDVI_g corresponds to bare soil (0.193), NDVI_∞ is the asymptotic value when Ω tends to infinity (limit reached when Ω is greater than 8.0), and K_{NDVI} controls the slope (an extinction coefficient). The values of K_{NDVI} and NDVI_∞ depend on the average leaf inclination (equal to 0.93 and 0.965 for average leaf inclination of 50°) [*Baret and Guyot*, 1991].

Manually digitized radar (MDR) is a program that produces a complete computer-generated composite map of the echo characteristics. These data have been generated using information from all the 100 radars around the country [*Moore and Smith*, 1979]. The data are presented as video integrator and processor (VIP) levels, which are the maximum levels for that particular grid box. These VIP levels are related to the rainfall rate (echo intensity is a function of precipitation), and MDR VIP levels 1, 2, 3, 4, 5, and 6 correspond to an echo intensity of light, moderate, heavy, very heavy, intense, and extreme. The VIP levels are converted into rain rates using conversion tables [*Fan et al.*, 1996], which take into account the geographical position of the MDR pixel, the month of the year, and the time of the day. The spatial and temporal resolution of the MDR data are 40 km and 1 hour, respectively [*Baeck and Smith*, 1995].

Soil type data for the Red River basin were available [*Abdulla et al.*, 1996]. Most of the Red River basin is composed of silt loam and loam soil. The Brooks-Corey parameters for a silt loam soil are $\theta_r = 0.02$, $\theta_s = 0.50$, $\psi(\theta_s) = 0.2$ m, $K_s = 1.89 \times 10^{-6}$ m s^{-1}, and m = 0.2 [*Rawls et al.*, 1982].

The TIROS operational vertical sounder (TOVS) has flown on NOAA spacecraft since 1978. The radiances observed by the high-resolution infrared sounder (HIRS2) and the brightness temperatures of the microwave sounding unit (MSU), the two sensors that make up TOVS, have been analyzed to provide daily fields of air temperature and humidity profiles, surface temperature, and cloud amounts and altitudes that occur [*Susskind et al.*, 1997]. These data sets are available as daily 1° × 1° gridded fields which we use in this study. The surface temperature is computed directly using the radiances from channels 8, 18, and 19 (the thermal channels) of the HIRS2 and the Planck equation. The surface air temperature and the specific humidity near the surface is obtained by extrapolating the air temperature profile and the specific humidity profile to the surface pressure level [*Susskind et al.*, 1984]. The data from NOAA 10 satellite for August 1, 1987, to July 31, 1988, are used here. The surface temperature is used for T_s^o; the surface air temperature and specific humidity are used for computing input forcings and various fluxes whenever they are available. When the satellite values are not available, (1) in the absence of T_s^o, assimilation is not carried out for the particular pixel and time period. (2) When air temperature and specific humidity are not available, the hourly values from the surface airways stations are used instead. NOAA 10 has a nadir 7:30 A.M./P.M. local time overpass at the equator. The observations at all other locations, north or south of the equator and all off-nadir observations, are at times different from 7:30 A.M./P.M. Since air and surface temperatures are very sensitive to time of day, the exact local time at each location was used in conjunction with the surface and air temperatures and the surface specific humidity. There are missing values in regions of excessive (80%) cloudiness. The TOVS surface temperature data have been shown [*Lakshmi and Susskind*, 2000] to have good agreement with the ground-based observations of surface temperature. The two estimates are unbiased (average difference over a long time period nearly equals zero), and the standard deviation of this bias is 3.5 K. These are excellent comparison characteristics when we take into account that the satellite is observing over an area and the ground measurements are point in nature. Finally, the TOVS satellite data are available 4 times a day (2:30 A.M./P.M. and 7:30 A.M./P.M.), which gives us a good diurnal characterization of the land surface temperature.

3.3. Observed Versus Simulated Surface Temperatures

The TOVS-derived surface temperatures corresponding to the NOAA 10 A.M. and P.M. overpasses averaged over the entire Red-Arkansas grid box (approximately 5° × 10°) are shown as a scatterplot (Figure 3) against the corresponding hydrological model–simulated surface temperature. Each point in the plot represents an instantaneous value. The value of the simulated surface temperature corresponding to each 1° × 1° grid box for the simulation corresponds to the exact time of overpass of the satellite over that grid box. The scatterplot shows that the mean difference between the satellite surface temperature and the model surface temperature (bias) is 1.77°C for the morning overpass and −3.67°C for the evening overpass. The correlation between the satellite and the model-simulated surface temperatures is high (0.97 for the morning overpass and 0.98 for the evening overpass). The standard deviation of the difference between the satellite surface temperature and the model-simulated surface temperature is 2.5°C and 1.79°C for the morning and evening overpasses, respectively. The slope of the best fit line gives an indication of the range of the two data. Slope values of less than unity mean that the model-simulated surface temperature has a lower range (maximum minus minimum) than the satellite surface temperature. This is the case for both the morning and evening satellite overpasses.

The comparison of the model-simulated diurnal cycle with the TOVS-derived surface temperature is shown in Figure 4 for four different days (one in each season, fall, winter, spring, and summer) in the year-long study period for a 1° × 1° pixel centered at 33°30′N, 99°30′W. The simulated surface temperature differs from the satellite observations by at most a few degrees. The difference between the TOVS-derived and the simulated surface temperatures for September 10, 1987, is 2.2°C for the morning overpass of the satellite and −3.9°C for the evening overpass. The corresponding numbers for December 12, 1987, March 11, 1988, and June 21, 1988, are 2.8°C, 4.0°C, and 4.4°C, respectively, for the morning satellite overpass and −4.4°C, −5.3°C, and 1.1°C, respectively, for the evening overpass. It is seen that the difference between the satellite and the simulated surface temperatures is positive in the morning overpass (satellite surface temperature is warmer) and is negative corresponding to the evening overpass (the model surface temperature is warmer). The only exception is the June 21, 1988, evening overpass when the difference is

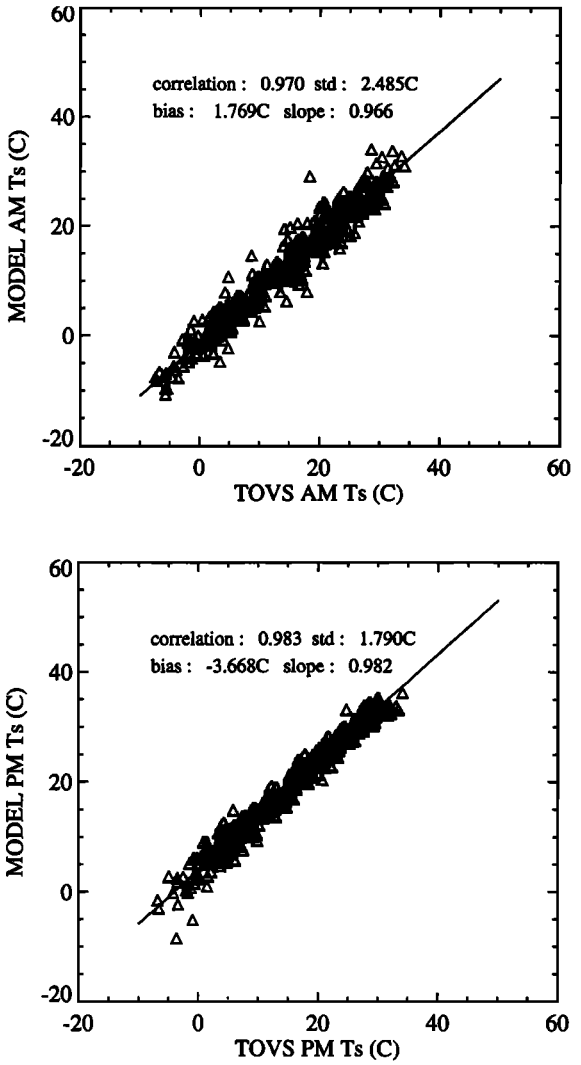

Figure 3. Comparison of the area-averaged model-generated and satellite-observed surface temperature corresponding to the morning and evening overpass of NOAA 11 for the Red River basin grid box over 1 year (August 1987 to July 1988).

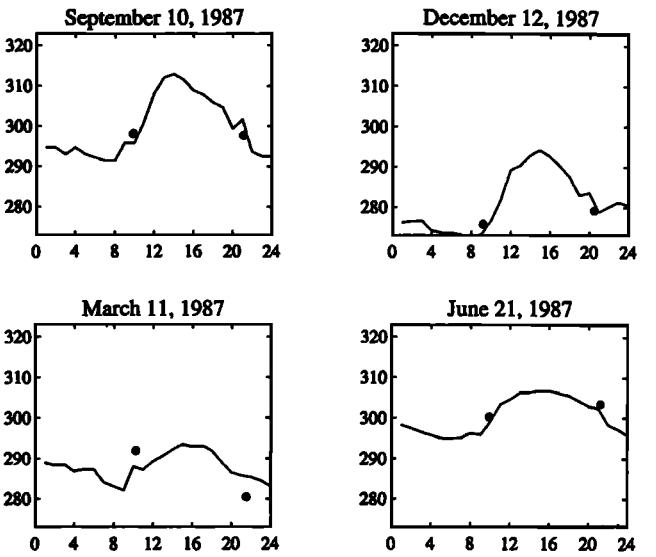

Figure 4. Comparison of model-computed diurnal cycle of surface temperature and the satellite-retrieved surface temperature from NOAA 10 for a 1° × 1° pixel centered at 33°30'N, 99°30'W for 4 days.

positive (the model is cooler). The model-simulated diurnal cycle shows a realistic seasonal pattern with warmer temperatures in the months of September and June and cooler temperatures in December and March. The diurnal cycle of the surface temperature shows a maximum around noon and minimum around 8:00 A.M. This comparison gives us a good idea of the relationship of the model-simulated data and the twice a day satellite retrieval. These comparisons over various seasons provide us with an idea of seasonal variability of the differences.

Plate 2a examines the spatial distribution of the mean and standard deviation of the satellite and model-simulated surface temperature difference. Temporal averaging of all morning and evening overpasses from August 1, 1987, to July 31, 1988, has been carried out for this result. The mean (temporal) bias (satellite minus model) is positive in the morning overpass (satellite warmer) with values ranging from 0.625°C to 3.94°C. The mean bias is predominantly negative for the evening overpass (satellite cooler) with the values ranging from −4.72°C to 0.107°C. This is consistent with the results of the four individual days (shown in Figure 4) which fall within these ranges. The temporal standard deviation, however, is always positive and ranges between 4.05°C and 5.59°C for the morning overpass and 3.06°C and 4.61°C for the evening overpass. The range in the mean bias is larger than the range in the standard deviation for both the morning and the evening satellite overpasses. In the morning overpass the bias is greater in a small zone running north-south in the center of the study area (around 4 K). The lower bias is seen in the edges of the study area (−1 K to 1 K), and the other areas fall roughly between these two bias values (2 K to 4 K) predominantly in the western portion of the study area. In the evening overpass the pixels of greatest bias are spread out in the east and the northwest. The spatial pattern for standard deviation does not exhibit distinct spatial patterns.

The comparison between the satellite surface temperature and the model-simulated surface temperature for an individual day (March 11, 1988) is shown in Plate 2b. The TOVS A.M. and P.M. overpasses are generally not "complete" (i.e., there are missing values for many pixels) over the study area. The model simulations are carried out for every pixel. The differences (satellite minus model) are absent for the pixels where TOVS surface temperatures are not available. This nonavailability could be due to excessive cloudiness (retrievals are not performed beyond 80% cloudiness) and/or orbit precession (wherein a spot is missed on a particular orbit). The difference between the satellite and the model surface temperature ranges between −8.21°C and 9.62°C for the morning overpass and −10.77°C and 8.44°C for the evening overpass. It is seen that the highest values of these differences occur in the west central portions of the study area in the morning overpass and central portion of the study area in the evening overpass. The differences generally have opposite signs between the morning and evening overpasses (positive for morning and negative for evening, similar to Figure 4). Most of the pixels show differences between −4°C and 0°C for the evening overpass and between 3°C and 8°C for the morning overpass. The differences between the satellite and the model surface temperatures are larger for a single day case (May 11, 1989) as com-

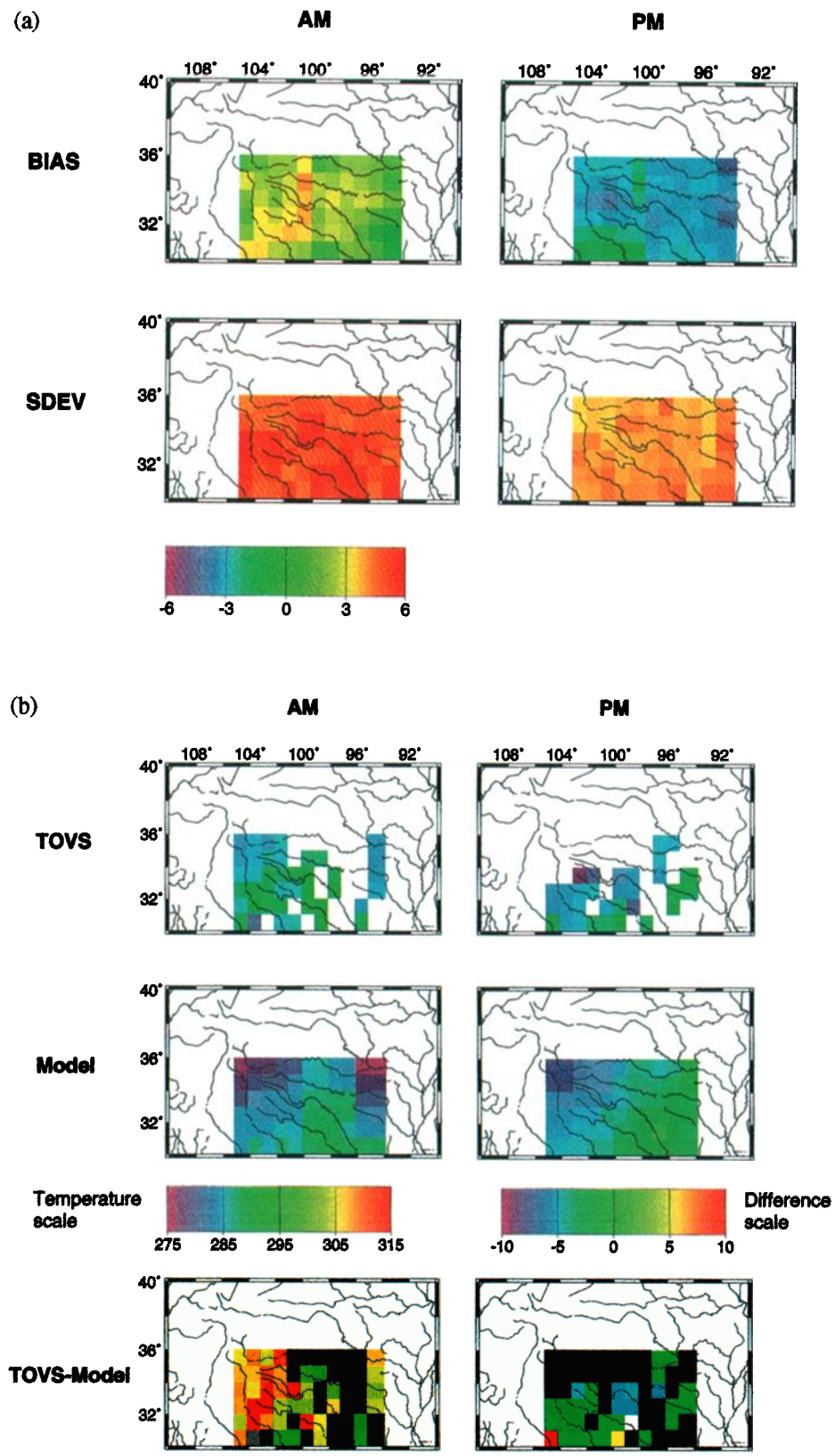

Plate 2. (a) Spatial distribution of the surface temperature bias (satellite minus model) and standard deviation of the bias for NOAA 10 A.M. and P.M. overpasses for the period between August 1, 1987, and July 31, 1988. (b) Spatial distribution of the surface temperature retrieved by TIROS operational vertical sounder (TOVS), model-computed surface temperature, and the differences for the A.M. and P.M. overpasses on March 11, 1988.

pared to the averages over the entire year which are smaller because of the averaging effect (compare Plate 2).

4. Soil Moisture Adjusted by Surface Temperature Assimilation

The assimilation scheme described in section 2 is tested using a series of experiments. The land surface hydrological model is run in two modes, namely, without assimilation of satellite surface temperature data and with the assimilation of satellite surface temperature. The data input into the hydrological model described in section 3.2 are treated as "perfect" inputs (described in section 3.2). The hydrological model is run along with this set of inputs with and without surface temperature assimilation. In addition to this set of runs the hydrological model is run with the "perfect" inputs perturbed. Perturbation is carried out for precipitation and the shortwave radiation as they have the most impact (of all the atmospheric inputs) on the land surface hydrological cycle. The precipitation affects the land surface moisture storage through the infiltration and the runoff and the upper and the lower layer soil moistures. The shortwave radiation is the driving force for the evapotranspiration during the sunlight hours. The precipitation and the shortwave radiation are biased 20% higher, 20% lower, and randomly using a random number between 0 and 1. In the runs where precipitation is biased, all the other inputs are unchanged (this includes the shortwave radiation) and vice versa. The only exception to this is one set of runs in which both the precipitation and the shortwave radiation are randomly perturbed simultaneously. The corresponding runs with and without surface temperature assimilation are compared. We simulate (continuously) hourly hydrological states, i.e., soil moisture, surface temperature, and all the heat and moisture fluxes. At the time step the TOVS surface temperature becomes available to us, we assimilate it using the relationship in (6). Therefore we do not carry out assimilation in the 12 hours between the two overpasses. In the present study, when satellite data are absent, no assimilation is carried out. There is no spatial or temporal interpolation of satellite data. The statistics for availability of data for the boxes for a year are as follows. The percentage of coverage (365 observations would mean complete coverage for the 7:30 A.M. orbit or 7:30 P.M. orbit, so percentage of 365 is expressed) for the 7:30 A.M. orbit ranges from 69 to 77%; for the 7:30 P.M. orbit the percentage ranges from 60 to 73%, and for the total (A.M. plus P.M. 100% means 730 observations) it ranges between 60 and 74%. The percentages presented above vary spatially between individual 1° grid boxes.

4.1. Comparison of Adjusted Soil Moisture With Special Sensor Microwave Imager (SSM/I) Observations

The observed soil moisture for the Red River basin study area is computed using the 19-GHz brightness temperatures from the SSM/I for its ascending orbit (local overpass time approximately 6:00 A.M.). A canopy radiative transfer model and an atmospheric attenuation model have been used to retrieve the surface soil moisture by subtracting the canopy and the atmospheric contributions to the observed satellite brightness temperatures [*Lakshmi et al.*, 1997b]. The SSM/I-derived soil moistures are completely independent of this hydrological model and the TOVS surface temperature as neither is used in the retrieval process. The top panel in Plate 1b shows the cumulative difference (in millimeters) between the 1-cm-layer model-simulated soil moisture from the SSM/I observations of soil moisture for the case without surface temperature assimilation and the SSM/I observations of soil moisture and 1-cm model-simulated soil moisture with surface temperature assimilation for two cases of precipitation bias, i.e.,

$$\text{Cumulative difference} = \Sigma[(|W_{\text{ssmi}} - W_{na}|) - (|W_{\text{ssmi}} - W_a|)], \quad (16)$$

where W_{ssmi} is the soil moisture derived from the ascending orbit of the SSM/I, W_{na} is the soil moisture simulated by the model for the case with no surface temperature assimilation, and W_a is the soil moisture simulated with surface temperature assimilation. The center and bottom panels of Plate 1b show the effect of surface temperature assimilation on the cases of +20% rainfall bias ($1.2P$) and −20% rainfall bias ($0.8P$) for the surface soil moisture. These results are presented in Plate 1b for the 66 1° × 1° boxes for the Red River basin. The effect of assimilation of surface temperature is to improve the agreement of the model-simulated surface soil moisture with the SSM/I-retrieved soil moisture by as much as 7.0 mm over the November 1987 to August 1988 time period. The reduction in the time period for the comparisons is due to the fact that the previous study [*Lakshmi et al.*, 1997b] used the period August 1, 1987, to October 31, 1987, to calibrate the brightness temperature retrieval algorithm. Therefore the SSM/I brightness temperatures are used to retrieve the soil moisture using the calibrated parameters from November 1, 1987, to July 31, 1988. There is significant improvement in the northeastern corner (7.09 mm), south central (6.27 mm), and most of the west central region (ranging between 3.02 mm and 6.27 mm). Most of the study region shows an improvement in the range of 0–3 mm. A few 1° × 1° grid boxes show a decline in the performance with assimilation; these range from −0.1 mm to −0.61 mm.

The effect of the precipitation bias is to change the soil moisture of the model. This effect is a complex one, and it is not always a simple case of increased rainfall leading to increased soil moisture. In the case of high incoming solar and longwave radiation this increased moisture could result in increased evaporation or in cases of a large precipitation event; the effect of high soil moisture would be to increase the runoff for the time steps subsequent to the precipitation event. Therefore a simple cause-effect relationship cannot be formulated between the increased precipitation and soil moisture. It can be seen from Plate 1b that the improvement in the soil moisture of the top layer due to assimilation ranges from 0 to 7.0 mm for the positive and the negative rainfall bias cases. The regions of most improvement due to surface temperature assimilation correspond to the regions which have the largest difference between the model-computed surface temperature and the TOVS-retrieved surface temperature. This can be observed by comparing Plates 1b and 2a. The region in the northeast corner which shows the largest improvement (7.23 mm and 6.99 mm for the $0.8P$ and the $1.2P$ cases, respectively) corresponds to a bias (−4 K to −6 K) in the TOVS P.M. overpass. The central region in the two cases where improvements range from 4 mm to 6 mm corresponds to the same region in the TOVS A.M. overpass where the bias ranges between 3 K and 5 K. It is clear that the regions where the temperatures differ the most correspond to the largest changes in the adjusted soil moisture. This adjusted soil moisture is in closer agreement with the independent set of soil moisture estimates from the SSM/I than the unadjusted (no surface

Table 2. Improvement in Areal Average Upper Layer Soil Water Compared to SSM/I Retrievals due to Assimilation of Surface Temperature

Experiment	Improvement, mm
no change in inputs	2.18
−20% precipitation	2.22
+20% precipitation	2.14
−20% shortwave radiation	2.25
+20% shortwave radiation	2.12
random precipitation	2.19
random shortwave radiation	2.20
random precipitation and shortwave radiation	2.21

temperature assimilation) soil moistures. This proves our assertion that the assimilation of surface temperatures rectifies the errors caused due to incorrect precipitation estimation. Table 2 shows the spatial average of the cumulative improvements (as shown in Plate 1b) for all the cases run with and without surface temperature assimilation for different perturbations of precipitation and radiation inputs. The improvement is represented as a spatial average, ranging from 2.1 mm to 2.2 mm. This shows that the assimilation of surface temperature is a definite improvement for accurate simulation of the surface soil moisture.

4.2. Comparison of Adjusted Soil Moisture With Simulated Control

In order to fully explore the potential of the surface temperature assimilation, we carried out more comparisons of the soil moisture field adjusted by surface temperature assimilation with the unadjusted soil moisture field for cases of input rainfall biased by +20% and −20%. The simulated observations are taken to be the soil moisture fields corresponding to the perfect (unperturbed) inputs along with surface temperature assimilation. Plate 1c shows the bias and the standard deviation of the difference: simulated observations minus perturbed rainfall soil moisture field with and without assimilation. This is shown for both the rainfall bias cases ($0.8P$ and $1.2P$). It can be seen from Plate 1c that the effect of assimilation is to reduce the bias to close to zero. This is true for both the increased rainfall ($1.2P$) and the decreased rainfall ($0.8P$) cases. The bias for the soil moisture field without assimilation is high, ranging between −0.006 and 0.001 (volumetric soil moisture) for the −20% rainfall input bias and between −0.001 and −0.007 for the +20% rainfall input bias. The corresponding values of bias are close to 0.0005 or less for both the cases after assimilation of surface temperature. The improvement in the standard deviation is also apparent from the lower panels in Plate 1c. The difference in the standard deviation between the $0.8P$ and $1.2P$ and the simulated observations decreases from 0.005–0.020 for no assimilation to 0.0001 with assimilation in both the cases. This result is significant as it demonstrates that the effect of assimilation is not only to improve the mean difference between the observations and the model simulations but also the day-to-day variability of the simulations. The time variation of the area-averaged bias and standard deviation differences from the control case is shown in Figures 5 and 6, respectively. The upper layer spatial mean and spatial standard deviation of the volumetric soil moisture are depicted in the top panels (Figures 5 and 6, respectively) for the control case with and without surface temperature assimilation. It can be seen that in the case of no changes in the input, assimilation of surface temperature does not result in any significant differences between the two cases of soil moisture for spatial mean and standard deviation. In Figure 5, the middle and bottom panels show the difference between the area-averaged soil moisture for the control case with assimilation and the rainfall bias cases ($0.8P$ and $1.2P$, respectively) with and without assimilation. It is seen that the perturbed input rainfall cases with assimilation case differences in soil moisture are closer to zero compared to the case without assimilation. The same is true with the soil moisture standard deviation. The standard deviation difference between the control with assimilation and the perturbed rainfall input simulated soil moistures shows a better agreement for the surface temperature assimilation case (middle and bottom panels of Figure 6). The time series of these differences shows that the assimilation case is very close to zero for both bias and standard deviation and varies temporally for the case without assimilation.

Even though many sensitivity experiments were examined, detailed presentation was limited only to those experiments related to precipitation perturbation. Precipitation is the most important input to hydrological models. Incorrect precipitation estimation not only causes incorrect computed soil moisture but also incorrect fluxes of moisture, infiltration, runoff, and base flow, and fluxes of energy, evapotranspiration flux, surface temperature (and hence), sensible ground heat flux, and net radiation. Therefore precipitation is the most important and the least well known (especially spatial distribution) variable and forms the central theme in the discussions in this paper. The purpose of having these precipitation bias experiments is to prove that in the presence of incorrect precipitation input (which will result in incorrect soil moistures), the assimilation of observed surface temperature helps to bring the soil moisture toward the "correct" value. This is physically consistent with the fact that the soil moisture and surface temperature are not independent of each other but are connected intimately through the coupling of the energy and water budgets by evapotranspiration.

5. Discussion and Conclusions

Unlike measurements of surface temperature, routine observations of soil moisture are rare. Field experiments measure soil moisture at limited spatial scales and over limited time periods. Therefore validation of model-simulated soil moisture is virtually nonexistent at regional spatial scales and over temporal scales of months to years. This paper attempts to reconcile the absence of routine soil moisture observations by using the more readily observed surface temperatures to validate model surface temperatures and subsequently "adjust" model-simulated soil moistures.

The surface temperature assimilation presented in this paper adjusts the model-simulated surface soil moisture based on the difference between the model-simulated and observed surface temperature and at the same time preserves the water and energy balance at the land surface. This innovative method has been shown to produce better predictions of soil moisture especially when the rainfall and/or radiation inputs are in error. This result has been verified using SSM/I-retrieved soil moisture observations which are completely independent of the simulation and assimilation schemes as well as the TOVS-observed surface temperature. In addition, simulation experiments that use the hydrological model to produce "observa-

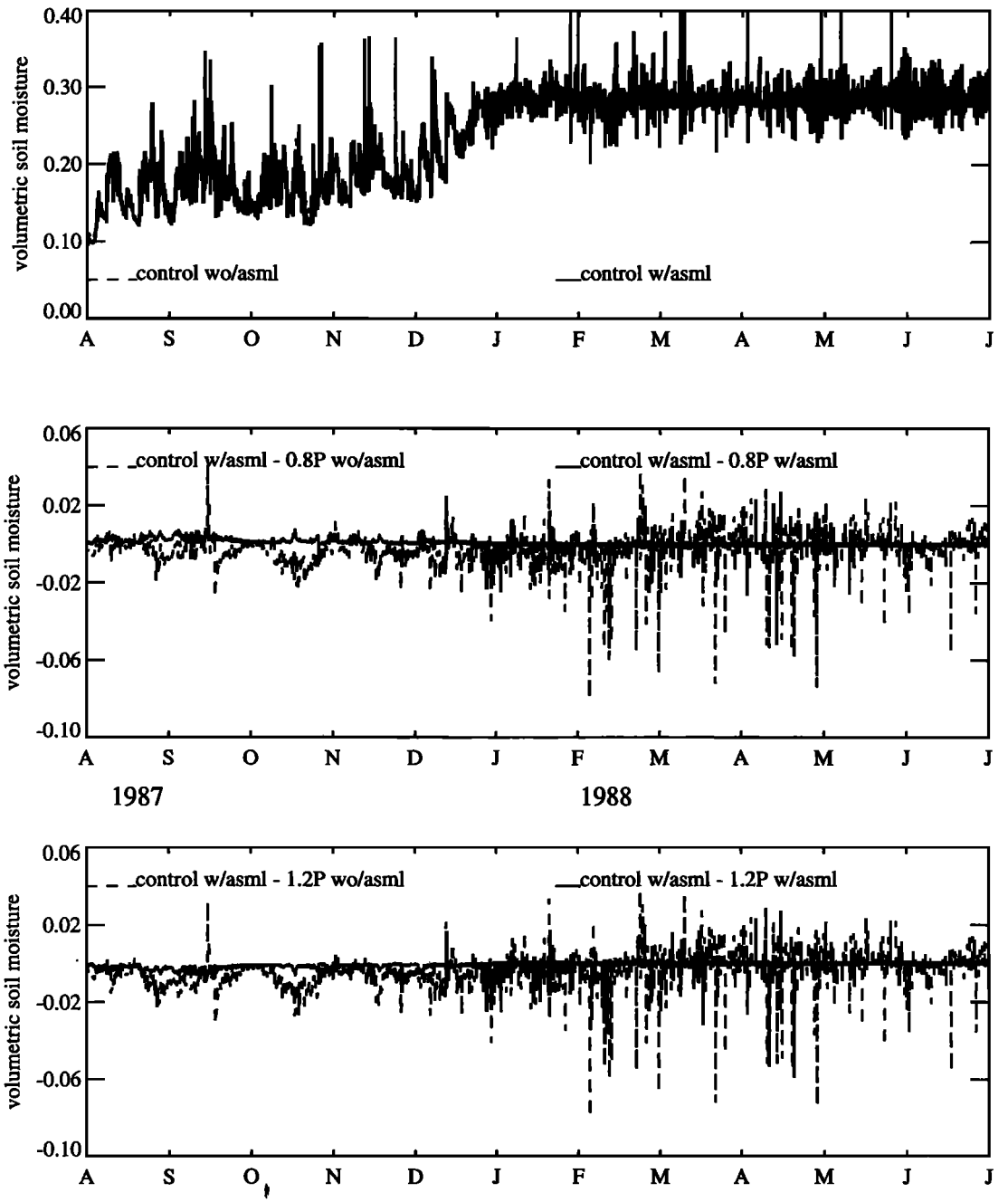

Figure 5. Temporal evolution of the upper layer volumetric soil moisture averaged over the Red-Arkansas grid box between August 1, 1987, and July 31, 1988, for the (top) control with and without assimilation cases, (middle) difference between the spatial average control with assimilation and the rainfall input biased 20% lower with and without assimilation, and (bottom) difference between the spatial average control with assimilation and the rainfall input biased 20% higher with and without assimilation.

tions" of soil moisture using the unperturbed inputs are used to compare with the hydrological model-simulated soil moisture with perturbed inputs with and without surface temperature assimilation. The comparisons show that the assimilation of surface temperature not only reduces the bias (or the difference between the observed and simulated soil moistures) but also the standard deviation of the difference.

The choice of a simple average of model-simulated and satellite-retrieved T_s for the assimilated surface temperature T_s' is based on results from previous studies. *Lakshmi and Wood* [1998] showed that long-term simulations of the surface temperature using a two-layer hydrological model exhibit a bias of 1.7 K and a standard deviation of difference of 4.3 K with the field measurements of surface temperature. This study corresponds to the First International Satellite Land Surface Climatology Project Field Experiment (FIFE) conducted in the prairie grasslands of Kansas in 1987–1989 [*Hall and Sellers*, 1995]. *Lakshmi et al.* [1997a, 1997b] used the thin-layer model (described in this paper) to show that the model-simulated surface temperatures differed from the field measurements by a bias of 1.5 K and a standard deviation of 4.8 K. Both these studies are based on the grassland regions of Kansas and not

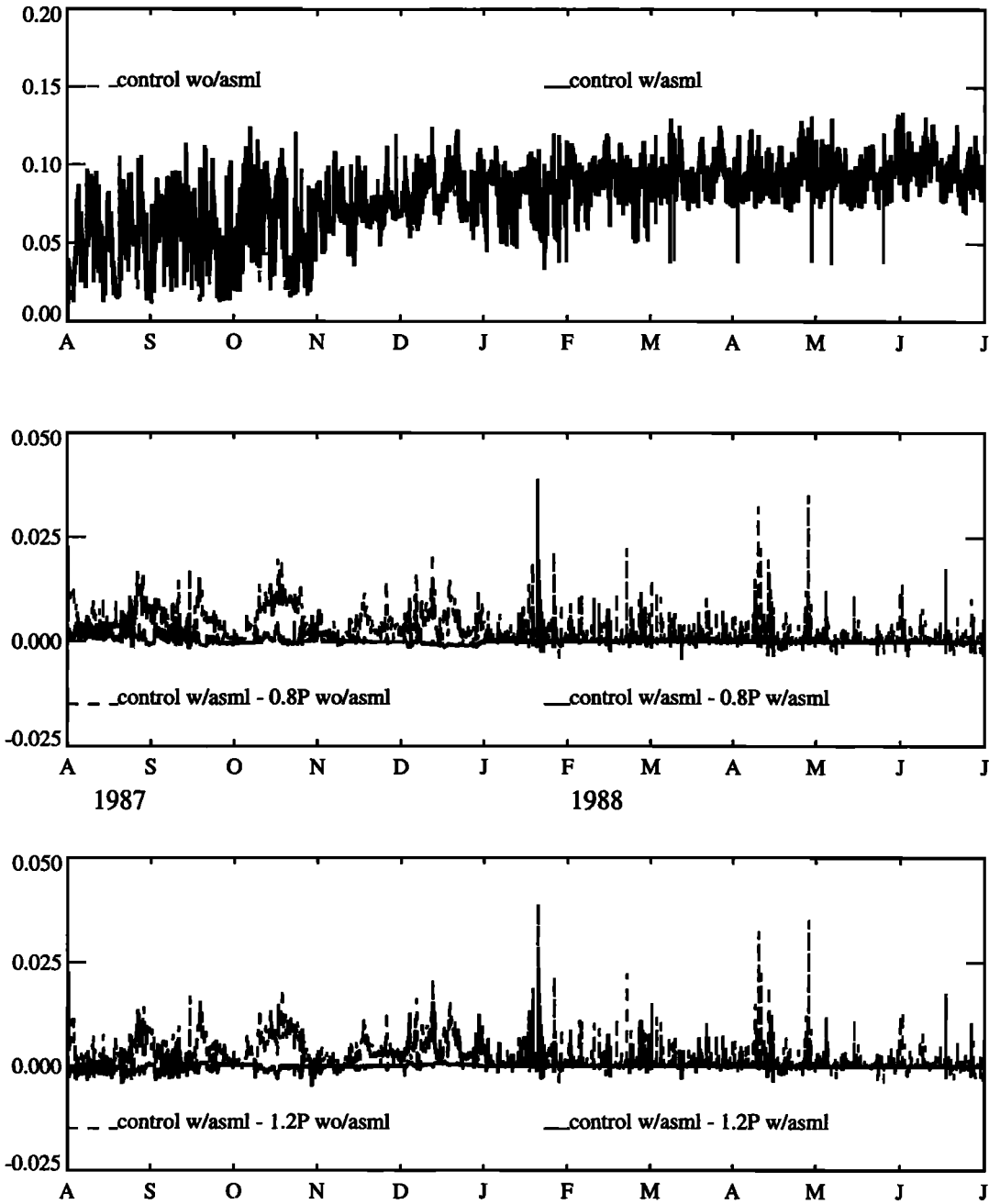

Figure 6. Temporal evolution of the upper layer volumetric soil moisture spatial standard deviation over the Red-Arkansas grid box between August 1, 1987, and July 31, 1988, for the (top) control with and without assimilation cases, (middle) difference between the spatial standard deviation control with assimilation and the rainfall input biased 20% lower with and without assimilation, and (bottom) difference between the spatial standard deviation control with assimilation and the rainfall input biased 20% higher with and without assimilation.

on the present study region, as field measurements of surface temperature were not available for this region. However, the two regions are quite similar with respect to land surface cover type, and these results can be used. Another interesting fact with the above two results is that the difference between the field measurements and the model-simulated surface temperature estimates seem to be independent of the model used. This indicates a "limit" on model abilities to accurately simulate these measurements.

Lakshmi and Susskind [2000] have compared TOVS satellite-retrieved surface temperatures with field measurements for various locations (Kansas, United States of America; Sahel, Africa; and boreal forests, Canada). It is seen that the bias and the standard deviation for Kansas (FIFE) are 1.3 K and 4.7 K, respectively. In fact, the other regions (Sahel and boreal forests) show remarkably similar statistics to the FIFE region.

In the light of these results I find it very convincing to assume equal weights for satellite retrievals and model estimates of surface temperature in constructing an assimilated surface temperature.

The amount of "adjustment" in soil moisture for the cases of imperfect precipitation inputs does involve other factors. This means that incorrect wind speed or leaf area index cannot be individually accounted for in the updating of soil moisture. All the discrepancies, in model formulation, model parameters, and input data, are taken into account in this assimilation scheme. However, in these experiments ($0.8P$ and $1.2P$), precipitation bias is the largest source of discrepancy, and it is the major factor in the adjustment of soil moistures. In most assimilation schemes, after assimilation of data, the water and/or energy budgets are not preserved. This is not so in the present case. In the case of the water budget we change the upper layer soil moisture and the bare soil evaporation. Therefore we have to adjust the runoff to reflect this change. The runoff is decreased/increased to keep a perfect water balance; that is, precipitation equals change in upper layer soil moisture plus bare soil evaporation plus runoff plus exchange flux. The exchange flux $q_{1,2}$ is changed at the time step after updating. Therefore the water budget is preserved in this assimilation scheme. The energy budget is preserved by recalculating the outgoing longwave radiation (using the new surface temperature), sensible heat flux, and ground heat flux.

The assimilation scheme presented in this paper is simple and completely general in nature, i.e., independent of the hydrological model structure. It is not specific to the thin-layer model which has been used in this study. A similar formulation can be used for a three-layer or multilayer soil model.

This assimilation study will lead to future studies that will assimilate more than one hydrological variable into land surface and coupled land-atmosphere models. The hydrological variables that can be assimilated include soil moisture (when observations are available) and streamflow data. There are numerous spatial and temporal issues with these observations and processes that will have to be resolved before such a task is undertaken. The resulting general assimilation scheme will provide an excellent framework for complete utilization of all land surface observations and satellite-retrieved observations in improving hydrological predictions.

Acknowledgments. This work has been funded by the Land Surface Hydrology Program at NASA Headquarters; Program Scientists were Dennis Lettenmaier (1997–1998) and Eric Wood (1998–1999). The author wishes to thank them for their continued support. The use of TOVS data has been made possible by the Sounder Research Team (Joel Susskind, Team Leader), and computer support was provided by Paul Piraino.

References

Abdulla, F. A., D. P. Lettenmaier, E. F. Wood, and J. A. Smith, Application of a macroscale model to estimate the water balance for the Arkansas-Red River basin, *J. Geophys. Res.*, *101*(D3), 7449–7459, 1996.

Baeck, M. L., and J. A. Smith, Climatological analysis of manually digitized radar data for the United States east of the Rocky Mountains, *Water Resour. Res.*, *31*(12), 2035–2045, 1995.

Baret, F., and G. Guyot, Potentials and limits of vegetation indices for LAI and APAR assessment, *Remote Sens. Environ.*, *35*, 161–173, 1991.

Blyth, K., The use of microwave remote sensing to improve spatial parameterization of hydrological models, *J. Hydrol.*, *152*, 103–129, 1993.

Bouttier, F., J.-F. Mahfouf, and J. Noilhan, Sequential assimilation of soil moisture from atmospheric low-level parameters, I, Sensitivity and calibration studies, *J. Clim.*, *32*, 1335–1351, 1993a.

Bouttier, F., J.-F. Mahfouf, and J. Noilhan, Sequential assimilation of soil moisture from atmospheric low-level parameters, II, Implementation in a mesoscale model, *J. Clim.*, *32*, 1352–1364, 1993b.

Brutsaert, W., *Evaporation Into the Atmosphere, Theory, History and Applications*, 299 pp., D. Reidel, Norwell, Mass., 1982.

Diak, G. R., Evaluation of heat flux, moisture flux and aerodynamic roughness at the land surface from knowledge of PBL height and satellite derived surface temperatures, *Agric. For. Meteorol.*, *52*, 181–198, 1990.

Dozier, J., and J. Frew, Rapid calculation of terrain parameters for radiation modeling from digital elevation data, *IEEE Trans. Geosci. Remote Sens.*, *28*, 963–969, 1990.

Eagleson, P. S., *Dynamic Hydrology*, 462 pp., McGraw-Hill, New York, 1970.

Entekhabi, D., H. Nakamura, and E. G. Njoku, Solving the inverse problem for soil moisture and temperature profiles by sequential assimilation of multifrequency remotely sensed observations, *IEEE Trans. Geosci. Remote Sens.*, *32*, 438–448, 1994.

Fan, Y., E. F. Wood, M. L. Baeck, and J. A. Smith, Fractional coverage of rainfall over a grid: Analyses of NEXRAD data over the Southern Plains, *Water Resour. Res.*, *32*(9), 2787–2802, 1996.

Feyen, J. C., and D. Hillel, Comparison between measured and simulated plant water potential during soil water extraction by potted rye grass, *Soil Sci.*, *129*, 180–185, 1980.

Gates, W. L., et al., An overview of the results of the Atmospheric Model Intercomparison Project (AMIP I), *Bull. Am. Meteorol. Soc.*, *80*(1), 29–55, 1999.

Goward, S. N., S. Turner, D. G. Dye, and S. Liang, The University of Maryland improved Global Vegetation Index product, *Int. J. Remote Sens.*, *15*(17), 3365–3395, 1994.

Hall, F. G., and P. J. Sellers, First International Satellite Land Surface Climatology Project (ISLSCP) Field Experiment (FIFE) in 1995, *J. Geophys. Res.*, *100*(D12), 25,383–25,395, 1995.

Henderson-Sellers, A. J., K. McGuffie, and A. J. Pitman, A project for intercomparison of land surface parameterization schemes (PILPS) 1992 to 1995, *Clim. Dyn.*, *12*(12), 849–859, 1996.

Idso, S. B., A set of equations for full spectrum and 8- to 14-μm and 10.5- to 12.5-μm thermal radiation from cloudless skies, *Water Resour. Res.*, *17*(2), 295–304, 1981.

Lakshmi, V., and J. Susskind, Comparison of TOVS-derived land surface variables with ground observations, *J. Geophys. Res.*, *105*(D2), 2179–2190, 2000.

Lakshmi, V., and E. Wood, Diurnal cycles of evaporation using a two-layer hydrological model, *J. Hydrol.*, *204*, 37–51, 1998.

Lakshmi, V., E. F. Wood, and B. J. Choudhury, A soil-canopy-atmosphere model for use in satellite microwave remote sensing, *J. Geophys. Res.*, *102*(D6), 6911–6927, 1997a.

Lakshmi, V., E. F. Wood, and B. J. Choudhury, Evaluation of special sensor microwave imager satellite data for regional soil moisture estimation over Red River Basin, *J. Appl. Meteorol.*, *36*, 1309–1328, 1997b.

Mahrt, L., and H. Pan, A two-layer model of soil hydrology, *Boundary Layer Meteorol.*, *29*, 1–20, 1984.

McLaughlin, D., Recent developments in hydrologic data assimilation, *U.S. Natl. Rep. Int. Union Geod. Geophys. 1991–1994, Rev. Geophys.*, *33*, 977–984, 1995.

McNider, R. T., A. J. Song, D. M. Casey, P. J. Wetzel, W. L. Crosson, and R. M. Rabin, Towards a dynamic-thermodynamic assimilation of satellite surface temperature in numerical atmospheric models, *Mon. Weather Rev.*, *122*, 2784–2803, 1994.

Miller, D. A., and R. A. White, A conterminous United States multilayer soil characteristics data set for regional climate and hydrology, *Earth Interact.*, *2*(1), pap. 2, 1998.

Moore, P. L., and D. L. Smith, Manually digitized radar data—Interpretation and application, *NOAA Tech. Memo. NWS SR-99*, Natl. Ocean. and Atmos. Admin., Silver Spring, Md., 1979.

Ottle, C., and D. Vijal-Madjar, Assimilation of soil moisture inferred from infrared remote sensing in a hydrological model over the HAPEX-MOBILHY region, *J. Hydrol.*, *158*, 241–264, 1994.

Price, J. C., Land surface temperature measurements from the split window channels of the NOAA-7 advanced very high resolution radiometer, *J. Geophys. Res.*, *89*(D5), 7231–7237, 1984.

Rawls, W. J., D. L. Brakensiek, and K. E. Saxton, Estimation of soil water properties, *Trans. Am. Soc. Agric. Eng.*, *25*, 1316–1320, 1982.

Susskind, J., J. Rosenfield, and D. Reuter, Remote sensing of weather and climate parameters from HIRS2/MSU on TIROS-N, *J. Geophys. Res.*, *89*(D3), 4677–4697, 1984.

Susskind, J., P. Piraino, L. Rokke, L. Iredell, and A. Mehta, Characteristics of the TOVS Pathfinder Path A data set, *Bull. Am. Meteorol. Soc.*, *78*(7), 1449–1472, 1997.

Tennessee Valley Authority, Heat and mass transfer between a water surface and the atmosphere, *Lab. Rep. 14*, Knoxville, Tenn., 1972.

van den Hurk, B. J., W. Bastiaanssen, H. Pelgrum, and E. Meijgaard, A new methodology for assimilation of initial soil moisture fields in weather prediction models using Meteosat and NOAA data, *J. Appl. Meteorol.*, *36*, 1271–1283, 1997.

V. Lakshmi, Department of Geological Sciences, University of South Carolina, Columbia, SC 29208. (vlakshmi@geol.sc.edu)

(Received May 10, 1999; revised July 3, 2000;
accepted July 7, 2000.)